ADVANCED FUNCTIONAL MATERIALS
www.afm-journal.de

Materials Views
www.MaterialsViews.com

Mechanism for Efficient Photoinduced Charge Separation at Disordered Organic Heterointerfaces

*Harm van Eersel, René A. J. Janssen, and Martijn Kemerink**

Despite the poor screening of the Coulomb potential in organic semiconductors, excitons can dissociate efficiently into free charges at a donor–acceptor heterojunction, leading to application in organic solar cells. A kinetic Monte Carlo model that explains this high efficiency as a two-step process is presented. Driven by the band offset between donor and acceptor, one of the carriers first hops across the interface, forming a charge transfer (CT) complex. Since the electron and hole forming the CT complex have typically not relaxed within the disorder-broadened density of states (DOS), their remaining binding energy can be overcome by further relaxation in the DOS. The model only contains parameters that are determined from independent measurements and predicts dissociation yields in excess of 90% for a prototypical heterojunction. Field, temperature, and band offset dependencies are investigated and found to be in agreement with earlier experiments. Whereas the investigated heterojunctions have substantial energy losses associated with the dissociation process, these results suggest that it is possible to reach high dissociation yields at low energy loss.

1. Introduction

A simple back of the envelope calculation suggests that organic solar cells should not work efficiently, even in case a donor-acceptor (bulk) heterojunction[1] is used to facilitate charge generation. In organic solar cells absorption of a photon creates an exciton in either of the two semiconductor materials that diffuses to the donor-acceptor interface to form a charge transfer (CT) state across the interface that subsequently dissociates into a free hole and electron that are transported and collected at the electrodes. Conceptually the most critical and possibly limiting step seems the dissociation of the CT state. The prediction of a low free electron-hole generation yield follows from the low dielectric constant of organic semiconductors, typically $3 < \varepsilon_r < 4$. The Coulomb binding energy therefore exceeds the thermal energy ($k_BT \approx 25$ meV at room temperature) for electron-hole separations up to the thermal capture radius of around 14–20 nm. Since the inter-site distance in disordered organic semiconductors is a few nm at most, even electron-hole pairs that are a few sites apart should most likely not dissociate into free carriers unless a strong electric field is applied. In reality, however, organic solar cells have reached efficiencies up to 10%, recently.[2,3] Moreover, their performance is mainly limited by voltage losses and imperfect spectral overlap rather than by forming charges from absorbed photons. Experimentally, internal quantum efficiencies (IQE) in excess of 75% are found for many heterojunctions.[4–11] Since the IQE is defined as the extracted charge per absorbed photon under short circuit conditions, it accounts not only for dissociation or geminate recombination losses at the heterointerface, but also for losses related to exciton diffusion to the interface[5] and to bimolecular recombination and diffusion.[12] The cited high IQE values are therefore a lower limit for the actual charge generation yield. In organic bulk heterojunctions (oBHJ) the exciton dissociation efficiency is commonly assumed to be close to unity, provided that the phase separation is sufficiently intimate such that the exciton diffusion length is larger than the domain size. Regarding losses associated with bimolecular recombination and diffusion, drift-diffusion modeling has yielded contradictory estimates, ranging from a few percent only[13–15] to tens of percent for systems with low charge carrier mobility and/or unfavorable morphology.[12,16] The discrepancy between anticipated low and measured high yields for creating free photogenerated electrons and holes is well known, and has inspired a significant amount of research.[17–21] The most commonly employed framework to explain the high electron-hole dissociation yield is based on the Onsager[22] and Braun[23] models in which it is assumed that a field- and temperature-dependent dissociation process competes with non-radiative recombination of the electron-hole pair in the CT state. Although successful in describing experimental data, electron-hole pair lifetimes in the microsecond range are typically needed to make a quantitative fit to current-voltage characteristics.[14,15,21,24–26] Measured lifetimes are typically in the nanosecond range[27–31] although a value of 40 ns has been reported for an all-polymer system.[32] Proposed alternative dissociation mechanisms evoke hot carriers,[18] quantum confinement,[19,20] delocalization,[20,21] and disorder.[33] At electric fields that correspond to typical short circuit conditions, these models either predict low dissociation yields[18,33] or need to make stringent assumptions regarding carrier effective masses,[19] effective lifetime of the CT polaron pair,[21] or delocalization

H. van Eersel, Prof. R. A. J. Janssen, Dr. M. Kemerink
Eindhoven University of Technology
Department of Applied Physics
P.O. Box 513, NL-5600 MB
Eindhoven, The Netherlands
E-mail: m.kemerink@tue.nl

DOI: 10.1002/adfm.201200249

length.[20,21] The problem of electron-hole pair dissociation via thermally activated tunneling (hopping) under influence of an electric field and temperature in an energetically disordered landscape is ideally suited for a treatment with kinetic Monte Carlo (MC) techniques.[21,34–42] These works differ significantly in the assumed morphologies and in the energetic landscape in which disorder may be absent,[36,41] correlated,[42] or completely random. Nevertheless, generally the calculated recombination rates are low and strongly field- and temperature-dependent at typical short circuit fields unless rather extreme values for parameters like the junction field[36] or recombination rate[38–41] are used. Here, we use a two-step approach to the problem of electron-hole dissociation at disordered heterointerfaces. First, we determine the electron and hole hopping parameters by fitting to temperature-dependent current-voltage characteristics of unipolar devices. These parameters are subsequently used as input for a kinetic MC model describing exciton dissociation. All input parameters of this model are therefore *a priori* known from independent experiments. We find dissociation yields in excess of 90% at room temperature and zero field. Driven by the band-offset at the heterointerface, the photo-created exciton first transforms into a CT complex which subsequently dissociates into free charges. The mechanism underlying the latter process is a gradual relaxation into the disordered DOS, which enables the hopping carriers to overcome their mutual Coulomb attraction. For the investigated junctions the entire process is associated with substantial energy losses. The modeling suggests, however, that it is possible to design a junction with realistic parameters that dissociates excitons with high (≥75%) yield and modest (~0.1 eV) associated energy loss.

2. Model

We focus on the well-characterized system of MDMO-PPV:PCBM, blended in 1:4 weight ratio. For this system, temperature-dependent electron- and hole-only space-charge limited current vs. voltage (SCLC) curves are available.[43–45] The $I(V,T)$ curves were simultaneously fitted by a least-squares procedure using a commercial drift-diffusion solver.[46] The physics of hopping in a disorder-broadened Gaussian DOS are included via a mobility functional. Here, the mobility μ depends on temperature T and the (local) charge density and electric field F according to parameterized expressions taken from ref. [47]. Mobility and diffusion constant are connected via the generalized Einstein equation. The fitting procedure yields the parameters for the hopping transport: the attempt frequency ν_0, the width of the Gaussian DOS σ and the nearest neighbor distance a_{NN}. In brief, the fitting procedure uses deviations from perfectly quadratic SCLC behavior, in combination with the temperature dependence of the curves, to make statements about the details of the charge transport using the theoretical framework of the co-called extended Gaussian disorder model (EGDM) developed by Pasveer *et al.*[54] The complete set of $I(V, T)$ curves for each material is fitted simultaneously to yield ν_0, σ and a_{NN}.

The hopping parameters are input for the kinetic Monte Carlo program that is used to calculate dissociation and recombination yields. The program works on either a simple cubic lattice or an FCC lattice and only considers nearest neighbor hops. Hopping rates between an initial state i with energy E_i and a final state f with energy E_f are calculated as

$$\nu_{if} = \begin{cases} \nu_0 \exp\left(-\frac{E_f - E_i \pm q\vec{r}_{if}\cdot\vec{F} + \Delta E_C}{k_B T}\right) = \nu_0 \exp\left(-\frac{\Delta E}{k_B T}\right) (\Delta E > 0) \\ \nu_0 (\Delta E \leq 0) \end{cases} \quad (1)$$

where F is the external electric field, r_{if} the vector connecting initial and final sites, and q the positive elementary charge. The + (–) sign refers to electron (hole) hopping. The attempt frequency ν_0 includes the (constant) probability for tunneling between nearest neighbor sites and should be regarded as a success rate for downward hops. The term ΔE_C is the change in Coulomb energy $E_C = -q/(4\pi\varepsilon_0\varepsilon_r r_{eh})$ with $\varepsilon_0\varepsilon_r$ the dielectric constant (ε_r = 3.6) and r_{eh} the electron-hole distance. In order to avoid divergences at zero electron-hole separation, E_C is truncated at –0.5 eV. Although simplified, we note that for the parameters used, the expression for the Coulomb energy reproduces both the exciton binding energy of ~0.5 eV[48] as well as the CT binding energy that was estimated to be in the 0.1–0.2 eV range for this material combination and slightly higher for polymer blends.[49–51]

For each material the single-particle site energies E_i are drawn from a Gaussian distribution function

$$f(E_i) = \frac{1}{\sqrt{2\pi\sigma^2}} \exp\left(-\frac{(E_i - E_0)^2}{2\sigma^2}\right) \quad (2)$$

where E_0 is the average energy of the materials' HOMO or LUMO level. For MDMO-PPV we use $E^{LUMO}{}_0 = -3.0$ eV and $E^{HOMO}{}_0 = -5.2$ eV, and for PCBM $E^{LUMO}{}_0 = -4.1$ eV and $E^{HOMO}{}_0 = -6.1$ eV.[14,16]

When the electron and hole are on the same site, they form an exciton that can recombine with rate ν_{ex}, set to 10^9 s^{-1}.[52,53] Similarly, when on neighboring sites they form a CT complex that can recombine with rate ν_{CT}, taken 10^9 s^{-1}.[27–31]

The waiting time before an event (hop or recombination) occurs is calculated as[40]

$$\tau = -\frac{\ln(r)}{\Sigma_\nu} \quad (3)$$

where r is a random number drawn from a homogeneous distribution between 0 and 1 and Σ_ν is the sum of the rates of all possible events. The event that occurs after τ is selected randomly, using the rates of all possible events as weight factors. Energies, rates, and waiting time are updated after each hop. The material parameters used in the MC calculations are given in **Table** 1.

For the followed procedure, consistency of the MC model with the Pasveer model[47] on which the parameterized mobility functionals in the drift-diffusion solver are based is crucial and was explicitly checked. The MC model reproduces the low-density mobilities of Pasveer *et al.*[54] and Bouhasoune *et al.*[55] when the hopping parameters cited in ref. [54,55] are used as input.

Calculations are started by either generating a single exciton on a single (donor) site, or by generating an electron-hole pair in the CT state, with the hole (electron) on the donor (acceptor) side of the interface. The calculation ends when either the electron-hole pair recombines or when one of the

Table 1. Electron (PCBM) and hole (MDMO-PPV) transport parameters extracted from fitting the *I–V* curves in Figure 1 and used as input in the MC model.[a,b]

	PCBM	MDMO-PPV in oBHJ	Neat MDMO-PPV
ν_0 [$\times 10^{13}$ s^{-1}]	0.3 (0.04, 2)	0.008 (0.005, 0.02)	0.063
σ [eV]	0.12 (0.11, 0.13)	0.10 (0.085, 0.12)	0.14 (0.13, 0.15)
a_{NN} [nm]	2.54 (2.50, 2.58)	2.7 (2.4, 3.2)	1.6 (1.5, 1.7)

[a]The rightmost column lists the parameters for neat MDMO-PPV from ref. [54]; [b]The numbers between brackets indicate 95%-certainty intervals.

carriers reaches an edge of the box. Charges are generated in the middle of the box; box sizes are typically larger than twice the thermal capture radius. For each calculation point at least 5000 configurations were averaged. In order to avoid commensurability problems the lattice constant of the box was taken as the composition-weighted average of the donor and acceptor nearest neighbor distances.

Two types of morphology are used: a perfectly sharp donor-acceptor (DA) bilayer and a completely random DA mixture. These may be considered the extreme cases of realistic morphologies that are likely to have at least some degree of intermixing or even have several hierarchical length scales associated with phase separation. In case of the bilayer geometry, the electric field is applied perpendicular to the interface plane.

3. Results

Figure 1 shows the drift-diffusion fits to the temperature dependent SCLC data of electron-only PCBM devices (panel a) and hole-only devices with a 1:4 wt% blend of MDMO-PPV:PCBM as active layer; the corresponding parameters are given in Table 1. Within experimental accuracy the fits match the data. Hence, the relatively large uncertainties in the parameters are due to the limited temperature and voltage range over which the devices could be measured and fitted. However, the outcomes of the MC model presented below do not significantly change when these parameters are varied within their uncertainty margins. For comparison Table 1 also shows the parameters for neat MDMO-PPV as found in ref. [54]. The lower disorder and larger nearest neighbor distance for the same material in a bulk heterojunction are consistent with the well-known two order of magnitude increase in hole mobility upon of MDMO-PPV upon addition of PCBM to $\mu_{ho} \approx 1.4 \times 10^{-8}$ m^2/Vs.[44] For PCBM the electron mobility $\mu_{el} \approx 2 \times 10^{-7}$ m^2/Vs is essentially unaffected by the presence of 20 wt% MDMO-PPV, which is consistent with the existence of an (almost) pure acceptor phase in these blends, having a molecular packing that is not significantly affected by the blending.[44] It is therefore reasonable to use the hopping parameters of pure PCBM to describe the transport in the acceptor phase of these heterojunctions. It should be stressed that when both phases are mixed, as is typically the case in all-polymer cells, electron- and hole-only curves should be taken on the mixed active layer.

The hopping parameters $\sigma = 0.12$ eV and $a_{NN} = 2.5$ nm determined for PCBM differ from the values $\sigma = 0.07$ eV and $a_{NN} = 3.4$ nm that were extracted in ref. [43] from the same data. The reason is that the present analysis is based on the extended Gaussian disorder model,[47] whereas the previous one was based on a correlated-disorder model. In both cases, the nearest neighbor hopping distance a_{NN} is substantially larger than the physical distance between individual PCBM molecules of around 1.2 nm. Most likely, this enhancement is related to delocalization of the electron wavefunction over a few PCBM molecules.[56] The relatively high attempt frequency $\nu_0 = 3 \times 10^{12}$ s^{-1} is likely related to the rigidity of the C_{60} core of the PCBM molecule. The attempt frequencies found here are consistent with values obtained before using essentially the same methodology for pure PPV derivatives (see Table 1 and ref. [54,55]) and for a polyfluorene copolymer.[57] They are also similar to attempt frequencies used in ref. [39,40,42] but substantially higher than in ref. [35,37,38] when the latter are corrected for the tunneling probability.

Using the parameters extracted above to calculate yields for an idealized, i.e. perfectly sharp, heterojunction we find dissociation yields in excess of 90%, see **Figure 2**. Necessarily the field dependence is not very pronounced. Whether the charges are generated as exciton (dashed lines) at the DA interface or as CT pair (solid lines) across the interface has little effect, which is caused by the large LUMO and HOMO offsets between donor and acceptor, driving the efficient charge transfer. It is important to stress that this does not explain why the CT complex efficiently dissociates into free charges: even at 2.6 nm separation, i.e. the nearest neighbor distance, the Coulomb binding energy is more than six times k_BT. The mechanism underlying the CT dissociation will be discussed below.

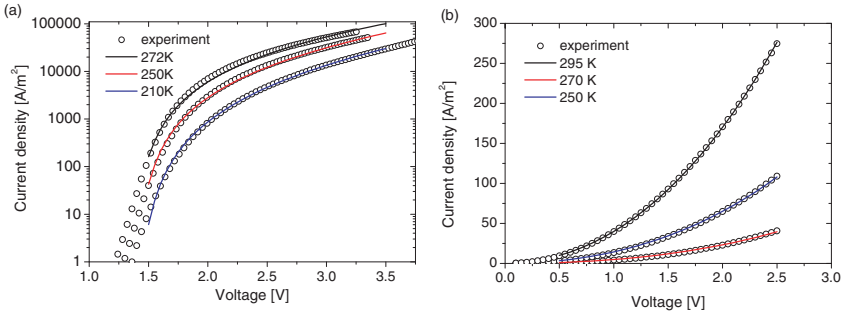

Figure 1. Temperature-dependent SCLC *I–V* curves of pure PCBM (a) and MDMO-PPV in an oBHJ mixed with 80 wt% PCBMS (b). Symbols are experimental data taken from ref. [43–45] and lines are drift-diffusion fits using the parameters listed in Table 1.

For MDMO-PPV:PCBM oBHJ it is well known that the donor-rich phase contains a significant (~50 wt%) fraction of well-dispersed acceptor material.[58] which is a characteristic feature of many polymer:PCBM oBHJs, even for some semi-crystalline polymers that form intercalated crystals with PCBM.[59] It is therefore likely that in these systems most of the charge generation actually occurs inside a mixed phase rather than at a sharp interface between two pure phases.[12,16] Figure 2b compares the yields for a bilayer system to those found for a random 1:1 (site density) blend. In order to rule out mobility effects the attempt frequencies

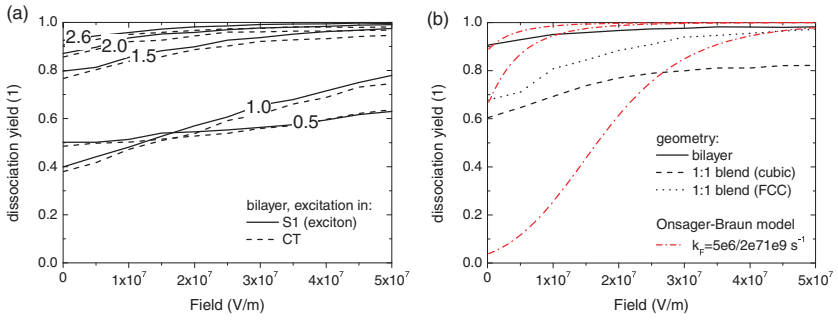

Figure 2. a) Dissociation yields vs. applied field calculated for a simple cubic bilayer system at room temperature. Solid (dashed) lines refer to excitation in the center of the donor exciton level (CT state). The nearest neighbor distance is varied and shown in the figure (in nm). b) As panel (a) for different geometries. Solid lines: bilayer, simple cubic lattice; dashed lines: random 1:1 blend, simple cubic lattice; dotted lines: random 1:1 blend, FCC lattice. Excitation is in the center of donor exciton level, the nearest neighbor distance is 2.6 nm. The red dash-dotted lines are calculated from the Braun/Onsager formula using Equation 4 (top to bottom) $\nu_{CT} = 5 \times 10^6$, 2×10^7, 1×10^9 s^{-1}. Modified calculation parameters to keep mobilities unchanged – random FCC blend: $\nu_0 = 2 \times 10^{11}$ s^{-1} (MDMO-PPV), $\nu_0 = 7.5 \times 10^{12}$ s^{-1} (PCBM); random simple cubic blend: $\nu_0 = 5 \times 10^{12}$ s^{-1} (MDMO-PPV), $\nu_0 = 2 \times 10^{14}$ s^{-1} (PCBM).

were rescaled such that the mobilities in the case of the random blends were equal to those in the pure phases of the bilayer. As anticipated, the escape yields in the random blends are lower than for the bilayer, which is due to a larger probability for the charges to get trapped or blocked by energetically inaccessible sites. Since the coordination number of the FCC lattice (12) is larger than that of the simple cubic lattice (6) this effect is most pronounced in the latter case. For bilayers the difference in yield between FCC and cubic is marginal (not shown). Nevertheless, the dissociation yield is substantially above 50% in all cases and less field dependent than reported in ref. [17] where an almost threefold increase at high fields was suggested.

The mechanism for the efficient dissociation of the CT complex into free charges can be understood from the relaxation dynamics of the electron and hole. **Figure 3**a shows the average energy vs. time of charge pairs that eventually escape. Energies are averaged over the charge carriers that are still present at a given time on the horizontal axis. Clearly, while the carriers relax into their respective DOS (black, red symbols) they overcome the Coulomb attraction (green triangles). The process is sketched in more detail on the left-hand side of **Figure 4**. The hole starts at zero energy (Figure 3a) because it has been created there. After charge transfer, the electrons on average sit at –1.1 eV, i.e. the LUMO offset, because that is the most likely energy to hop to. This step reduces the Coulomb binding energy from 0.5 eV to ~0.15 eV. Since both carriers are (on average) in the center of their respective DOS, they both 'see' a significant number of neighboring sites that represent a lower total energy: relaxation in the DOS overcomes the gain in Coulomb energy. For each successive hop the charges relax further in the DOS, but also move further apart, reducing the Coulomb binding. The right-hand side of Figure 4 shows a Jablonsky diagram of this process. It is important to note that since each (hopping) site has a single hole and single electron energy, relaxation in the DOS is only possible by moving to neighboring sites. There is no possibility for on-site relaxation. This mechanism differs fundamentally from the hot exciton mechanism that was proposed before.[18] In our work, hopping charges are assumed to immediately thermalize to the single particle energy of the local site. There is no local phonon bath of excess heat that can be used for the next hop. However, within the DOS formed by the ensemble of sites in the device/simulation the charges do thermalize, and do so by a process that slows down when charges are deeper in the DOS.[60] For the simulation shown in Figure 3a both charges have not yet completely thermalized within the DOS; the black and red arrows indicate equilibrium energies $E_\infty = \pm\sigma^2/k_BT$ for the hole (0.39 eV) and electron (–0.56 eV). In Figure 3, these are calculated with respect to the electron and hole starting energies in the center of the donor HOMO and donor LUMO levels, respectively. Hence, the electron reaches equilibrium at –(LUMO offset + 0.56) = –1.66 eV.

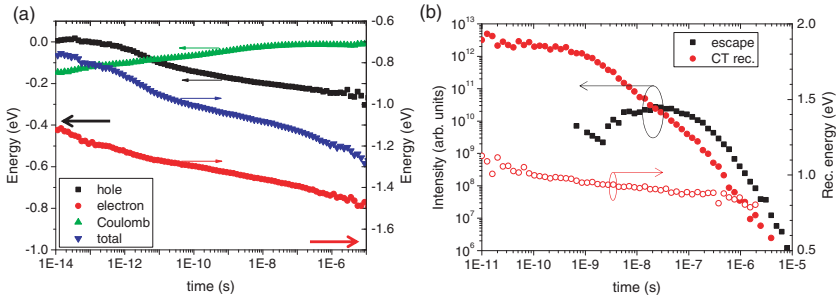

Figure 3. a) Average energy vs. time of charge pairs in a 1:1 random FCC blend that eventually escape. Energies are averaged over the charge carriers that are still present at a given time. Electron (hole) energies are calculated with respect to the center of the donor LUMO (HOMO) level, the total energy is calculated with respect to the energy in which the carriers have been excited, i.e., the center of the donor exciton level (S_1). The black and red arrows indicate the hole and electron equilibrium energy, respectively. b) Intensity of escape and CT recombination (left *y*-axis) and CT recombination energy (right *y*-axis). The dashed lines are guides for the eye. $F = 0$.

Also plotted in Figure 3a is the total energy of the system with respect to the S_1 exciton energy into which the charges were created (blue triangles). After charge transfer, the total energy relative to the S_1 exciton energy equals approximately $(E^{LUMO}{}_{0,\,PCBM} - E_{0,\,PPV}{}^{LUMO}) + (E^{exc}{}_B - E_B{}^{CT})$, i.e. the loss in LUMO energy plus the binding energy difference between exciton ($E^{exc}{}_B$) and CT ($E^{CT}{}_B$) state. It shows that there is a substantial energy loss associated with each of the two steps in the dissociation process described above. First, the negative offset at the shortest time is due to the fact that the offset between the LUMOs of donor and acceptor of 1.1 eV is roughly a factor three larger than the binding energy difference between the exciton and the CT complex. Second, the further decrease in total energy with time indicates that the relaxation

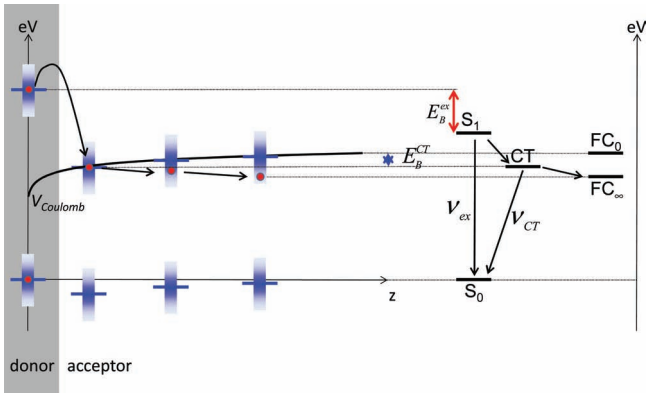

Figure 4. Left) Schematic representation of the two-step exciton dissociation process. Blue horizontal lines indicate the center of the donor and acceptor HOMO and LUMO levels, the vertical blue gradient bars indicate the broadened density of states. For illustrative purposes only the electron is assumed to move. Right) Corresponding Jablonsky diagram. After excitation in the donor S_1 level (red arrow indicates the exciton binding energy) the electron is transferred to, on average, the center of the acceptor LUMO, forming a CT complex. In subsequent downward hops, the electron relaxes towards its equilibrium energy while overcoming the remaining Coulomb energy (thick black line). Due to this relaxation the final energy of the free electron-hole pair FC_∞ is substantially below the "unrelaxed" free charge energy FC_0 defined as the donor-HOMO minus the acceptor LUMO energy.

Table 2. HOMO and LUMO energy levels and state energies for charge dissociation in MDMO-PPV:PCBM and a more energy efficient blend.

	HOMO [eV]	LUMO [eV]	Gap [eV]	Binding energy [eV]	State (S_1/CT/ FC_∞) energy [eV]
MDMO-PPV	–5.2	–3.0	2.2	0.5	1.7
PCBM	–6.1	–4.1	2.0	0.5	1.5
CT state	–5.2	–4.1	1.1	0.15	0.95
Relaxed charges	–4.81	–4.66	0.15	0	0.15
Donor 2	–5.2	–3.75	1.45	0.5	0.95
Acceptor 2	–6.1	–4.1	2.0	0.5	1.5
CT state 2	–5.2	–4.1	1.1	0.20	0.9
Relaxed charges	–5.06	–4.24	0.82	0	0.82

in the DOS overcompensates the increasing Coulomb energy. It should be kept in mind that in operational solar cells the charges relax to their respective quasi-Fermi levels which lie above the single particle equilibrium energies indicated by the arrows.[61] Hence, the total equilibrium energy loss calculated as the energy in which the charges are generated (the donor S_1 level) minus the total energy of the free, relaxed charges $((E^{LUMO}{}_{0,\ PCBM} + E_\infty el) - (E^{HOMO}{}_{0,\ PPV} + E_\infty hole)$that follows from this calculation (~1.55 eV) is an absolute upper limit: quasi-Fermi levels may lay substantially above the single particle equilibrium energies. Moreover, photogenerated charges may not completely thermalize within their (µs) lifetime. As described above the –1.55 eV drop in energy in this calculation comes from three contributions i) the loss in energy when going from S_1 to the CT state (–0.75 eV), ii) the Coulomb binding energy gained in the dissociation (0.15 eV), and iii) the loss in energy by carrier relaxation (–0.95 eV) (**Table 2**). Below we will show that in principle both losses can be reduced significantly, such that efficient dissociation can also be achieved with only ~0.13 eV of energy loss in the dissociation process.

The rate at which charges escape or recombine is plotted in Figure 3b. A number of characteristic time scales can be identified. The inflection point in the CT recombination intensity at 1 ns reflects the CT recombination rate set as input parameter; the decay at shorter times results from CT pairs being split up by one of the constituent charges hopping away. The inflection point in the escape rate around 0.2 µs reflects the time the fastest carrier–the electron–needs to diffuse to the boundary of the calculation box. Interestingly, the energy at which the CT states recombine decreases by ~0.2 eV over the time interval probed. This indicates that a significant fraction of the CT emission is due to electron-hole pairs that have first (partially) dissociated and are subsequently re-captured at a lower lying CT state.

In our model, exciton dissociation into CT states is described as the transfer of one charge to a neighboring site. Hence, this process occurs at a rate that is to good approximation equal to the average number of available downward hops times the attempt frequency. For a bilayer on a simple cubic lattice, where only one low-lying state (across the interface) is available for the electron, this gives an exciton dissociation rate of 3×10^{12} s^{-1}. For a random 1:1 blend on an FCC lattice the electron has, on average, 6 sites available, hence a dissociation rate of 2×10^{13} s^{-1} is obtained. The latter number is in reasonable agreement with experimentally observed quenching rates.[62]

We shall now return to the first step in the dissociation process, the charge transfer. From the discussion of Figure 3a it may be anticipated that roughly half the electron-hole pairs that are generated in the S_1 level dissociate into free charges when the difference between the exciton and CT binding energies of ~0.35 eV equals the LUMO offset, i.e. when the S_1 and CT energies are equal, see also Figure 4. The solid black line in

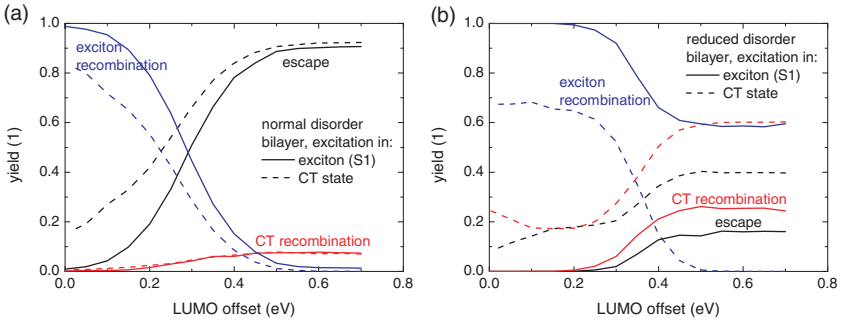

Figure 5. a) Yields at zero electric field vs. LUMO offset for a bilayer geometry on a simple cubic lattice. Black, red, and blue lines refer to escape, CT recombination, and exciton recombination yields, respectively. Solid (dashed) lines refer to excitation in the CT (donor exciton) level. b) As (a), for a situation with half the disorder. Parameters for the reduced-disorder calculation are $\nu_0 = 7 \times 10^8$ s^{-1} (MDMO-PPV), $\nu_0 = 4 \times 10^9$ s^{-1} (PCBM), keeping mobilities unchanged.

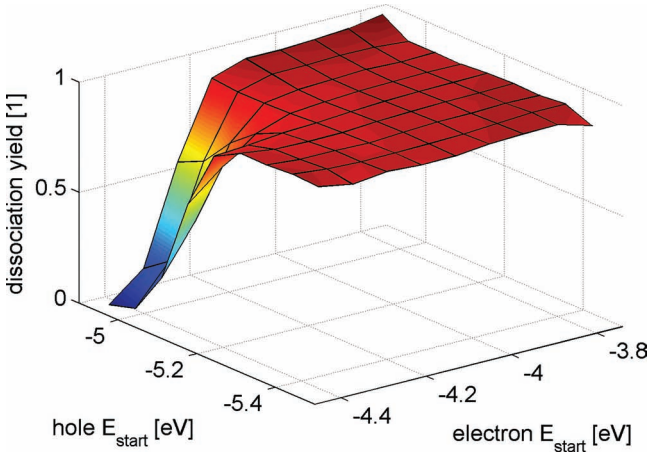

Figure 6. Dissociation yield vs. initial electron and hole energy. Excitation is in the CT state for a bilayer on a simple cubic lattice. The center of the donor HOMO and acceptor LUMO levels is at –5.2 and –4.1 eV, the considered energy window is $\pm 3\sigma$ for both electrons and holes.

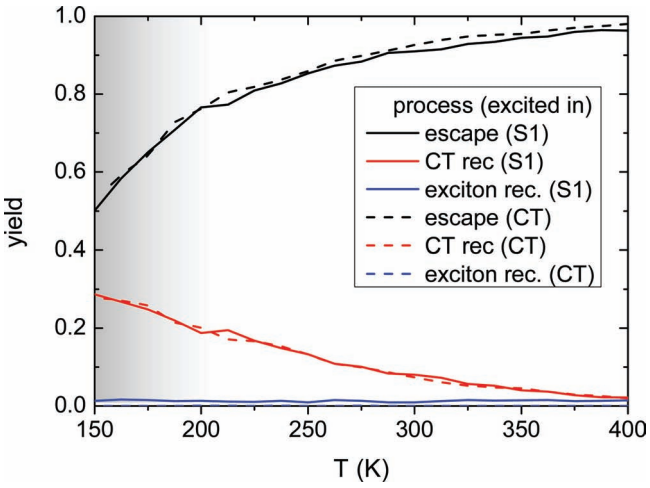

Figure 7. Yields at zero electric field vs. temperature for a bilayer geometry on a simple cubic lattice. Black, red, and blue lines refer to escape, CT recombination, and exciton recombination yields, respectively. Solid (dashed) lines refer to excitation in the center of the donor exciton (CT) level. Parameters are constant for all calculations. Below ~200 K the yields should be considered as lower limits.

Figure 5a shows that this is indeed the case. This finding supports the empirical rule of thumb that a ~0.3 eV LUMO offset is needed to drive charge transfer.[63] Expectedly, at low LUMO offsets direct excitation in the CT state leads to more efficient dissociation; at high offsets the yield is essentially equal for both excitation channels. The latter is in full agreement with experimental observations by Lee *et al.*, who found, for the MDMO-PPV:PCBM material system, that the IQEs for photoexcitation in the CT and exciton levels are equal.[9]

From the preceding discussion one may anticipate that the dissociation yield for excitation in the CT state strongly depends on the starting energy of the electron and hole. However, **Figure 6** shows that only when both the electron and the hole are created substantially (>σ) below the middle of their respective density of states a significant yield reduction results. The reason is that in all other cases at least one of the charges has sufficient possibilities to relax in the DOS, i.e. has neighboring sites of lower total energy, to still break up the CT exciton. This implies that for the present system the equivalence in terms of free charge generation of excitation in the S1 and CT levels holds for all excitation energies above roughly 0.9 eV (= CT gap - σ_e - σ_h). Due to the low joint DOS at these energies and the low optical cross section of the CT state in general, experimental observation of a reduced dissociation yield at such low excitation energies will be hard.

Interestingly, reducing the disorder, while maintaining the mobility via the attempt frequency, leads to a dramatic loss in dissociation efficiency, c.f. Figures 5a and b. This corroborates the importance of disorder in the dissociation process; reducing disorder reduces the number of final sites with a lower total energy, frustrating dissociation into free charges. It also shows that using a set of hopping parameters that produces a realistic mobility in an MC model is a necessary but insufficient condition to obtain a realistic description of the dissociation process. The specific values of all parameters are crucially important.

The temperature dependence of the IQE was studied by Lee *et al.*[9] They demonstrated that (a) the IQE is only weakly dependent on temperature, a threefold reduction when going from 300 K to 150 K was found, and (b) that the temperature dependence of the IQE for excitation in the S_1 and CT states was equal. Both observations are quantitatively reproduced by the simulations shown in **Figure 7**. As before (Figures 2, 5) the reason for the equal dissociation yields of S_1 (solid lines) and CT (dashed lines) excitation is the large LUMO offset in the MDMO-PPV:PCBM system of 1.1 eV. The limited temperature dependence is due to the fact that the splitting of the CT complex is driven by internal energy, i.e. the relaxation in the DOS, instead of by external (thermal) energy. In order to allow for direct comparison with Figure 3 and Supporting Information Figure S4a of ref. [9], in the calculation of Figure 7 all parameters, including the attempt frequency, are kept constant. The mobility therefore decreases with decreasing temperature. A consequence of the decreasing mobility is that at low temperatures a significant fraction of the electron-hole pairs does not recombine or dissociate within accessible calculation times due to trapping in deep states; at 200 K (150 K) this trapping is about 5% (20%). Hence, in this temperature window the plotted yields do not add up to unity and should be regarded as lower limits. The time evolution of the yields (not shown) suggests that most trapped charges will eventually escape.

So far, we have presented a quantitative explanation for the efficient generation of free charges from tightly bound excitons in oBHJs and bilayers. From Figure 3a it follows that this process is efficient, but at least in the case of MDMO-PPV:PCBM comes at the cost of a substantial energy loss. In the last part of this section we will investigate how this loss can be minimized. Figure 5 shows that the loss associated with the first step, the charge transfer, can be reduced to ~0.05 eV (i.e. the LUMO offset of ~0.4 eV minus the difference in binding energy between the S_1 and CT states of ~0.35 eV) without significant loss in dissociation yield. This is in full agreement with

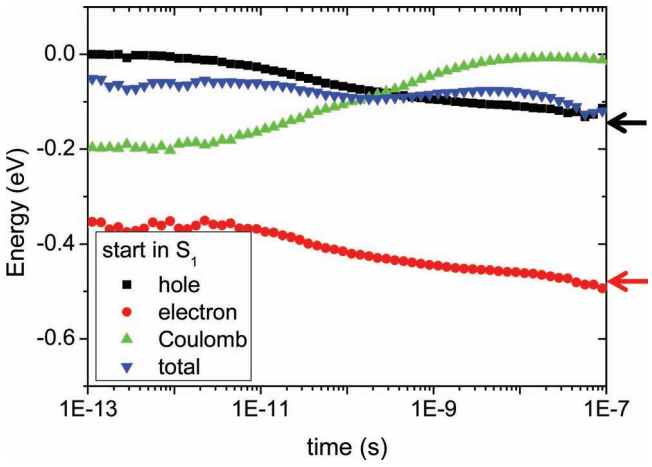

Figure 8. Average energy vs. time of charge pairs that eventually escape from a bilayer on a simple cubic lattice. Energies are averaged over the charge carriers that are still present at a given time. Electron (hole) energies are calculated with respect to the center of the donor LUMO (HOMO) level, the total energy is calculated with respect to the energy in which the carriers have been excited, i.e., the center of the donor exciton level (S_1). The black and red arrows indicate the hole and electron equilibrium energy, respectively. Material parameters have been optimized for minimal energy loss and are $\nu_0 = 1 \times 10^{11}$ s^{-1}; $\sigma_{HOMO} = \sigma_{LUMO} =$ 0.06 eV; $a_{NN} = 2$ nm; donor $E^{LUMO}{}_0 = -3.75$ eV and $E^{HOMO}{}_0 = -5.2$ eV; acceptor $E^{LUMO}{}_0 = -4.1$ eV and $E^{HOMO}{}_0 = -6.1$ eV; $F = 0$.

experimental data in ref. [64] where it was shown that photo-induced electron transfer from the lowest singlet excited state (S1) to the CT state occurs when E_{S1}-$E_{CT} > 0.1$ eV. However, the strong loss associated with the 'overrelaxation' in the DOS remains unaffected. The reason is simply that the sum of the electron and hole equilibrium energies $\left(\sigma_{ho}^2 + \sigma_{el}^2\right)/k_B T$ of ~1 eV largely exceeds the CT Coulomb binding energy of ~0.15 eV. Low energy loss therefore requires low disorder.[61] The ideal heterojunction therefore has a LUMO offset that equals the S_1–CT binding energy difference and allows the charges to relax just as much as needed to overcome the CT binding energy. In such an ideal heterojunction the sum of the LUMO offset and the energy relaxation equals the S_1 binding energy. In **Figure 8** we show the relaxation behavior of such an idealized heterojunction in bilayer geometry. The parameters used are shown in the caption and give rise to an electron and hole mobility of ~7×10^{-7} m^2/Vs. For comparison, the electron mobility in PCBM is ~2×10^{-7} m^2/Vs.[43] Hence, these parameters are optimistic but not completely unrealistic. Importantly, the resulting junction dissociates excitons into free charges with a yield of 74% at zero field and 300 K and with an associated total energy loss of ~0.13 eV (Table 2). Note that due to the low disorder and concomitant high mobilities, both electrons and holes have reached their equilibrium energy (±0.14 eV from their respective starting energies) after ~0.1 μs, as indicated by the arrows. Compared to the example of MDMO-PPV:PCBM the new parameters would lead to a -0.13 eV loss, again from three contributions i) the loss in energy when going from S_1 to the CT state (–0.05 eV), ii) the Coulomb binding energy gained in the dissociation (0.20 eV), and iii) the loss in energy by carrier relaxation (–0.28 eV) (Table 2).

The slight increase in total energy after ~1 ns in Figure 8 is due to the calculation of the total (and other) energies: they are average energies of the at a particular time still surviving electron-hole pairs. Typically, pairs that quickly relax also quickly dissociate or recombine. At later times these fast-relaxing pairs do no longer contribute to the average energy, which therefore increasingly reflects the not-so-fast relaxing, but still surviving pairs.

The calculation in Figure 8 should be regarded as an illustration that rational design of heterojunctions can prove worthwhile. It should be repeated that in operational solar cells charges relax to their respective quasi Fermi levels and not to their equilibrium energies.[61] Hence, the junction design should be such that under maximum power conditions, relaxation to the quasi Fermi levels provides sufficient driving force for the dissociation of the (unrelaxed) CT state.

4. Discussion

In this section we shall briefly discuss some aspects of the present findings in relation to previous work. Above, we have found a minor field dependence of the exciton to free charges dissociation yield, essentially because the yield at zero field is typically (far) above 50%. However, this does not imply that also CT recombination, or other loss channels, are also field independent. In contrast, in the simulations of Figure 2 the CT emission yield equals 100% minus the dissociation yield and does show pronounced field dependence. Hence, the field dependence of CT recombination, or other loss mechanisms, is not a proper measure for the (field dependence of the) exciton dissociation yield since already at zero field a significant fraction of excitons dissociates into free charges.[27]

The calculations presented above can be directly compared with the predictions from the Onsager/Braun formalism[22,23] which predicts the dissociation probability $P(F)$ to follow

$$P(F) = \frac{k_D(F)}{k_D(F) + k_F} \tag{4}$$

with k_F the CT recombination rate that is equal to $k_F = \nu_{CT} = 1 \times 10^9$ s^{-1} and k_D the field-dependent dissociation rate given by

$$k_D(F) = k_R \frac{3}{4\pi a_{NN}} \exp\left(-\frac{E_C(a_{NN})}{k_B T}\right) \frac{J_1\left(2\sqrt{-2b}\right)}{\sqrt{-2b}} \tag{5}$$

with k_R the Langevin recombination rate $k_R = q\left(\mu_{el} + \mu_{ho}\right)/\varepsilon_0\varepsilon_r$, $E_C(a_{NN})$ the Coulomb energy at the initial electron-hole separation distance, J_1 the Bessel function of the first kind and order 1, and $b = q^3 F / 8\pi\varepsilon_0\varepsilon_r k_B^2 T^2$. Since there is no distribution of initial separations here, $P(F)$ does not need to be averaged over such a distribution, as is commonly done when comparing with experiments.[17,27] Since all parameters in Equations 4 and 5 are known, $P(F)$ can straightforwardly be calculated. The result is shown by the lowest of the blue dash-dotted lines in Figure 2b. Clearly, the Onsager/Braun model yields a poor description of the actual MC result, irrespective of the particular geometry or lattice used in the MC calculation. In order to get $P(0)$ close to the MC values for the given parameters, recombination rates in the range $k_F = 10^6$–10^7 s^{-1} are needed ($k_F = 1 \times 10^9$ s^{-1} was used

in the MC calculations). As mentioned in the introduction, similar, unrealistically high values for k_F were found by using Equation 4 and 5 to fit experimental current-voltage characteristics.

In view of the results of previous kinetic MC calculations, the high dissociation yields found in the present work may appear surprising. A major factor is the value of the nearest neighbor distance a_{NN} = 2.6 nm in the present work, whereas values around 1 nm were typically used in previous works.[34,37,39–42] Using 1 nm in combination with the other parameters in the present work increases the CT binding energy from ~0.15 eV to ~0.4 eV, and concomitantly the zero-field yield decreases from ~90% to ~50% (Figure 2a). However, this value is still substantially higher than most previously reported values, indicating that a_{NN} is not the sole factor responsible for the high yields found here. This shows, again, that all parameter values matter and should ideally be experimentally determined from independent measurements.

Finally, we should stress that although the present model successfully reproduces a number of experimental findings related to photoinduced charge separation, extensions can be made, and are likely to be relevant for some, or even all material systems. Apart from the effects already discussed, one should think of including more realistic morphologies.[36,38–42] Alternatively, enhanced PCBM crystallization away from the heterointerface may provide an additional driving force for charge separation.[65]

5. Conclusions

We have presented a dynamical Monte Carlo study to exciton dissociation in organic bulk heterojunction solar cells. Unlike previous MC works, the parameters describing the charge carrier hopping were extracted from independent measurements. For this, space-charge limited current-voltage characteristics were fitted using a drift-diffusion model with parameterized expressions for the field- and density-dependent electron and hole mobility. The extracted parameters were used as input in the MC model which therefore only contained independently determined parameters.

The experimentally observed high efficiency for exciton dissociation is explained as a two-step process. Driven by the band offset, one of the carriers first hops across the interface, forming a charge transfer (CT) complex. Since the electron and hole forming the CT complex have typically not relaxed within the disorder-broadened density of states (DOS), their remaining binding energy can be overcome by further relaxation in the DOS. As this process is driven by the internal energy of the non-relaxed system the dissociation yield therefore only shows a moderate thermal activation and a weak dependence on electric field. Even under these conditions, in which, irrespective of electric field, the vast majority of excitons dissociates into free charges, we find that the (small) fraction of polaron pairs that do recombine is strongly field dependent. Hence, the field dependence of the polaron pair recombination yield is not a relevant measure for the exciton dissociation yield.

The investigated heterojunctions show that substantial energy losses are associated with the exciton dissociation process. However, our results suggest that it is possible to reach high dissociation yields at low energy loss with proper materials design.

Acknowledgements

The authors gratefully acknowledge L. J. A. Koster and M. M. Wienk for providing the transport data and P. A. Bobbert, R. Coehoorn, S. C. J. Meskers, and R. de Vries for stimulating discussions and suggestions. The work of H. v. E. is funded by the Dutch program NanoNextNL. This work was further supported by the "Europees Fonds voor Regionale Ontwikkeling" (EFRO) in the Interreg IV-A project Organext.

Received: January 26, 2012
Revised: March 4, 2012
Published online: April 16, 2012

[1] G. Yu, J. Gao, J. C. Hummelen, F. Wudl, A. J. Heeger, *Science* **1995**, *270*, 1789.
[2] R. F. Service, *Science* **2011**, *332*, 293.
[3] M. A. Green, K. Emery, Y. Hishikawa, W. Warta, E. D. Dunlop, *Prog. Photovolt: Res. Appl.* **2012**, *20*, 12.
[4] Y. Liang, Z. Xu, J. Xia, S.-T. Tsai, Y. Wu, G. Li, C. Ray, L. Yu, *Adv. Energy Mater.* **2010**, *22*, 135.
[5] G. F. Burkhard, E. T. Hoke, S. R. Scully, M. D. McGehee, *Nano Lett.* **2009**, *9*, 4037.
[6] G. Dennler, K. Forberich, M. C. Scharber, C. J. Brabec, I. Tomiš, K. Hingerl, T. Fromherz, *J. Appl. Phys.* **2007**, *102*, 054516.
[7] S. H. Park, A. Roy, S. Beaupré, S. Cho, N. Coates, J. S. Moon, D. Moses, M. Leclerc, K. Lee, A. J. Heeger, *Nat. Photonics* **2009**, *3*, 297.
[8] J. Meiss, K. Leo, M. K. Riede, C. Uhrich, W.-M. Gnehr, S. Sonntag, M. Pfeiffer, *Appl. Phys. Lett.* **2009**, *95*, 213306.
[9] J. Lee, K. Vandewal, S. R. Yost, M. E. Bahlke, L. Goris, M. A. Baldo, J. V. Manca, T. Van Voorhis, *J. Am Chem. Soc.* **2010**, *132*, 11878.
[10] H. Hoppe, N. Arnold, N. S. Sariciftci, D. Meissner, *Sol. Energy Mater. Sol. Cells* **2003**, *80*, 105.
[11] L. H. Slooff, S. C. Veenstra, J. M. Kroon, D. J. D. Moet, J. Sweelssen, M. M. Koetse, *Appl. Phys. Lett.* **2007**, *90*, 143506.
[12] K. Maturová, S. S. van Bavel, M. M. Wienk, R. A. J. Janssen, M. Kemerink, *Nano Lett.* **2009**, *9*, 3032.
[13] J. D. Kotlarski, P. W. M. Blom, L. J. A. Koster, M. Lenes, L. H. Slooff, *J. Appl. Phys.* **2008**, *103*, 084502.
[14] L. J. A. Koster, E. C. P. Smits, V. D. Mihailetchi, P. W. M. Blom, *Phys. Rev. B* **2005**, *72*, 085205.
[15] V. D. Mihailetchi, H. Xie, B. de Boer, L. J. Anton Koster, P. W. M. Blom, *Adv. Funct. Mater.* **2006**, *16*, 699.
[16] K. Maturová, S. S. van Bavel, M. M. Wienk, R. A. J. Janssen, M. Kemerink, *Adv. Funct. Mater.* **2011**, *21*, 261.
[17] V. D. Mihailetchi, L. J. A. Koster, J. C. Hummelen, P. W. M. Blom, *Phys. Rev. Lett.* **2004**, *93*, 216601.
[18] V. I. Arkhipov, E. V. Emelianova, H. Bässler, *Phys. Rev. Lett.* **1999**, *82*, 1321.
[19] V. I. Arkhipov, P. Heremans, H. Bässler, *Appl. Rev. Lett.* **2003**, *82*, 4605.
[20] V. Nenashev, S. D. Baranovskii, M. Wiemer, F. Jansson, R. Österbacka, A. V. Dvurechenskii, F. Gebhard, *Phys. Rev. B.* **2011**, *84*, 035210.
[21] C. Deibel, T. Strobel, V. Dyakonov, *Phys. Rev. Lett.* **2009**, *103*, 036402.
[22] L. Onsager, *Phys. Rev.* **1938**, *54*, 554.
[23] C. L. Braun, *J. Chem. Phys.* **1984**, *80*, 4157.

[24] V. D. Mihailetchi, H. Xie, B. de Boer, L. M. Popescu, J. C. Hummelen, P. W. M. Blom, L. J. A. Koster, *Appl. Phys. Lett.* **2006**, *89*, 012107.
[25] D. J. D. Moet, M. Lenes, J. D. Kotlarski, S. C. Veenstra, J. Sweelssen, M. M. Koetse, B. de Boer, P. W. M. Blom, *Org. Electron.* **2009**, *10*, 1275.
[26] D. J. D. Moet, M. Lenes, M. Morana, H. Azimi, C. J. Brabec, P. W. M. Blom, *Appl. Phys. Lett.* **2010**, *96*, 213506.
[27] D. Veldman, O. Ipek, S. C. J. Meskers, J. Sweelssen, M. M. Koetse, S. C. Veenstra, J. M. Kroon, S. S. van Bavel, J. Loos, R. A. J. Janssen, *J. Am. Chem. Soc.* **2008**, *130*, 7721.
[28] F. Etzold, I. A. Howard, R. Mauer, M. Meister, T.-D. Kim, K.-S. Lee, N. S. Baek, F. Laquai, *J. Am. Chem. Soc.* **2011**, *133*, 9469.
[29] J. M. Hodgkiss, A. R. Campbell, R. A. Marsh, A. Rao, S. Albert-Seifried, R. H. Friend, *Phys. Rev. Lett.* **2010**, *104*, 177701.
[30] A. Howard, R. Mauer, M. Meister, F. Laquai, *J. Am. Chem. Soc.* **2010**, *132*, 14866.
[31] J. Guo, H. Ohkita, H. Benten, S. Ito, *J. Am. Chem. Soc.* **2010**, *132*, 6154.
[32] S. Westenhoff, I. A. Howard, J. M. Hodgkiss, K. R. Kirov, H. A. Bronstein, C. K. Williams, N. C. Greenham, R. H. Friend, *J. Am. Chem. Soc.* **2008**, *130*, 13653.
[33] O. Rubel, S. D. Baranovskii, W. Stolz, F. Gebhard, *Phys. Rev. Lett.* **2008**, *100*, 196602.
[34] U. Albrecht, H. Bässler, *Chem. Phys. Lett.* **1995**, *235*, 389.
[35] T. Offermans, S. C. J. Meskers, R. A. J. Janssen, *J. Chem. Phys.* **2003**, *119*, 10924.
[36] P. Peumans, S. R. Forrest, *Chem. Phys. Lett.* **2004**, *398*, 27.
[37] T. Offermans, S. C. J. Meskers, R. A. J. Janssen, *Chem. Phys.* **2005**, *308*, 125.
[38] P. K. Watkins, A. B. Walker, G. L. B. Verschoor, *Nano Lett.* **2005**, *5*, 1814.
[39] R. A. Marsh, C. Groves, N. C. Greenham, *J. Appl. Phys.* **2007**, *101*, 083509.
[40] C. Groves, R. A. Marsh, N. C. Greenham, *J. Chem. Phys.* **2008**, *129*, 114903.
[41] M. Wojcik, P. Michalak, M. Tachiya, *Appl. Phys. Lett.* **2010**, *96*, 162102.
[42] C. Groves, J. C. Blakesley, N. C. Greenham, *Nano Lett.* **2010**, *10*, 1063.
[43] V. D. Mihailetchi, J. K. J. van Duren, P. W. M. Blom, J. C. Hummelen, R. A. J. Janssen, J. M. Kroon, M. T. Rispens, W. J. H. Verhees, M. M. Wienk, *Adv. Funct. Mater.* **2003**, *13*, 43.
[44] V. D. Mihailetchi, L. J. A. Koster, P. W. M. Blom, C. Melzer, B. de Boer, J. K. J. van Duren, R. A. J. Janssen, *Adv. Funct. Mater.* **2005**, *15*, 795.
[45] J. A. Koster, unpublished. Hole-only SCLC curves below room temperature were only available as parameters in the model used in ref. [43,44]. For this reason hole transport fits were made on a linear scale, which puts most weight on the high-current regime in which the parameterized expressions are most accurate.
[46] SETFOS 3.2 was used for the drift-diffusion fits. SETFOS is developed by FLUXiM, http://www.fluxim.com, (accessed March, 2012).
[47] R. Coehoorn, W. F. Pasveer, P. A. Bobbert, M. A. J. Michels, *Phys. Rev. B.* **2005**, *72*, 155206.
[48] Knupfer, *Appl. Phys. A.* **2003**, *77*, 623.
[49] M. Hallermann, S. Haneder, E. Da Como, *Appl. Phys. Lett.* **2008**, *93*, 053307.
[50] J. Kern, S. Schwab, C. Deibel, V. Dyakonov, *Phys. Status Solidi RRL* **2011**, *5*, 364.
[51] S. Gélinas, O. Paré-Labrosse, C. N. Brosseau, S. A. Seifried, C. R. McNeill, K. R. Kirov, I. A. Howard, R. Leonelli, R. H. Friend, C. Silva, *J. Phys. Chem. C* **2011**, *115*, 7114.
[52] D. E. Markov, C. Tanase, P. W. M. Blom, J. Wildeman, *Phys. Rev. B.* **2005**, *72*, 045217.
[53] V. Mikhnenko, F. Cordella, A. B. Sieval, J. C. Hummelen, P. W. M. Blom, M. A. Loi, *J. Phys. Chem. B* **2008**, *112*, 11601.
[54] W. F. Pasveer, J. Cottaar, C. Tanase, R. Coehoorn, P. A. Bobbert, P. W. M. Blom, D. M. de Leeuw, M. A. J. Michels, *Phys. Rev. Lett.* **2005**, *94*, 206601.
[55] M. Bouhassoune, S. L. M. van Mensfoort, P. A. Bobbert, R. Coehoorn, *Org. Electron.* **2009**, *10*, 437.
[56] H. Tamura, M. Tsukada, *Phys. Rev. B.* **2012**, *85*, 054301.
[57] S. L. M. van Mensfoort, S. I. E. Vulto, R. A. J. Janssen, R. Coehoorn, *Phys. Rev. B.* **2008**, *78*, 085208.
[58] J. K. J. van Duren, X. Yang, J. Loos, C. W. T. Bulle-Lieuwma, A. B. Sieval, J. C. Hummelen, R. A. J. Janssen, *Adv. Funct. Mater.* **2004**, *14*, 425.
[59] C. Miller, R. Gysel, C. E. Miller, E. Verploegen, Z. Beiley, M. Heeney, I. McCulloch, Z. Bao, M. F. Toney, M. D. McGehee, *J. Polym. Sci. B* **2011**, *49*, 499.
[60] W. Chr. Germs, J. J. M. van der Holst, S. L. M. van Mensfoort, P. A. Bobbert, R. Coehoorn, *Phys. Rev. B.* **2011**, *84*, 165210.
[61] J. C. Blakesley, D. Neher, *Phys. Rev. B.* **2011**, *84*, 075210.
[62] C. Brabec, G. Zerza, G. Cerullo, S. De Silvesri, S. Luzzati, J. C. Hummelen, S. Sariciftci, *Chem. Phys. Lett.* **2001**, *340*, 232.
[63] M. C. Scharber, D. Mühlbacher, M. Koppe, P. Denk, C. Waldauf, A. J. Heeger, C. J. Brabec, *Adv. Mat.* **2006**, *18*, 789.
[64] D. Veldman, S. C. J. Meskers, R. A. J. Janssen, *Adv. Funct. Mater.* **2009**, *19*, 1939–1948.
[65] F. C. Jamieson, E. Buchaca Domingo, T. McCarthy-Ward, M. Heeney, N. Stingelin, J. R. Durrant, *Chem. Sci.* **2012**, *3*, 485.